Chapter 13

Classification of Breast Density Patterns Using PNN, NFC, and SVM Classifiers

Indrajeet Kumar*, Jitendra Virmani†, Harvendra S. Bhadauria*, Manoj K. Panda* and Kriti‡
*G.B. Pant Engineering College, Pauri, Garhwal, India, †CSIR-CSIO, Chandigarh, India, ‡Thapar University, Patiala, India

ABBREVIATIONS

ROI	region of interest
CAD	computer-aided diagnosis
ANN	Artificial Neural network classifier
BIRADS	Breast Imaging Reporting and Data System
DDSM	Digital Database for Screening Mammography
MIAS	Mammographic Image Analysis Society
SBT	segmented breast tissue
HCF	hybrid classification framework
k-NN	k-nearest neighbors
MI	misclassified instances
SVM	support vector machine classifier
SFS	sequential forward search
NFC	neurofuzzy classifier
MLO/CC	Mediolateral oblique/Cranial Caudal
IFV	Input feature vector
CM	confusion matrix
OCA	overall classification accuracy
ICA	individual class accuracy
TI	testing instance
PNN	probabilistic neural network

1 INTRODUCTION

Cancer is a condition identified as an irrepressible multiplication of body cells resulting in accumulation of masses. These masses are termed as tumors and may be malignant or benign [1]. According to a study carried out by the American Cancer Society, it is estimated that among US women, the likelihood of developing breast cancer is 1 in 12 [2, 3]. The major risk factor of mounting breast lesions can be attributed to age, genetic history of breast cancer, implants, alcohol consumption, high density of the breast, etc.

The connection between the possibility of breast lesions and dense breast parenchyma has constantly been advocated by different researchers in their studies [4–11]. The American College of Radiology (ACR) introduced BIRADS as a universal reference according to which mammographic images can be bifurcated into different classes as per density information of the breast tissue [11–16]. Mammography is a screening tool that can be used in the initial phases for diagnosis of breast cancer during the asymptomatic stage when symptoms of breast cancer have not occurred [17–23]. Different density patterns exhibit different appearances on the mammograms. By observing a mammogram, the radiologist can assess the density patterns of the breast tissue and give a proper diagnosis. Breast tissue with low density appears dark, while a breast tissue with high density appears almost bright on a mammogram. The intermediate stage between low-density tissue and high-density tissue appears to be dark with scattered bright streaks. According to BIRADS, the breast tissue has been divided into four density classes:

Soft Computing Based Medical Image Analysis. https://doi.org/10.1016/B978-0-12-813087-2.00012-9

(a) BIRADS-I: B-I (Almost entirely fatty. Less than 25% glandular tissue is present).
(b) BIRADS-II: B-II (Some fibroglandular tissue. 25%–50% fibroglandular tissues scattered in the breast).
(c) BIRADS-III: B-III (Heterogeneously dense breast. 50%–75% of the breast tissue is dense).
(d) BIRADS-IV: B-IV (Extremely dense breast. More than 75% of the breast contains glandular tissue).

The sample images belonging to each BIRADS class taken from the Digital Database for Screening Mammography (DDSM) database have been presented in Fig. 1.

Sometimes, the density patterns exhibited by the breast tissue overlap each other thus making it difficult for the radiologist to predict the density of the breast tissue just on the basis of visual inspection. So it is highly recommended that if the prediction for suspicious cases is dense (B-III or B-IV), then such cases must be double screened for the presence of masked lesions. For such type of cases, the author used ImageJ software to enhance dense mammograms (by adjusting contrast and brightness) in order to detect the lesions. The sample of these cases taken from DDSM dataset is shown in Fig. 2.

Thus to overcome this problem and help the radiologists make a proper diagnosis, the researchers have developed different computer-aided diagnostic (CAD) [24–31] systems that discriminate the mammograms as per their density into one of the BIRADS classes using the texture properties of the images through machine-learning approach. In the present work, for the density classification of breast density, a framework is designed using probabilistic neural network classifier (PNN), Neurofuzzy classifier (NFC), and support vector machine (SVM) classifiers. It is well established that the PNN is a probability-based classifier, SVM is a supervised learning-based classifier, and NFC is a combination of neural network and fuzzy system.

A brief description of studies performed on the DDSM database for 4-class and 2-class breast density classification is summarized in Table 1A and B, respectively.

From Table 1, it cans be seen that the most of the studies were performed on DDSM dataset for breast density classification using SBT- and ROI-based approach. The highest classification accuracy of 90.8% has been achieved for 4-class classification of breast density based on ROI approach [39], while 94.0% is also achieved for SBT-based approach.

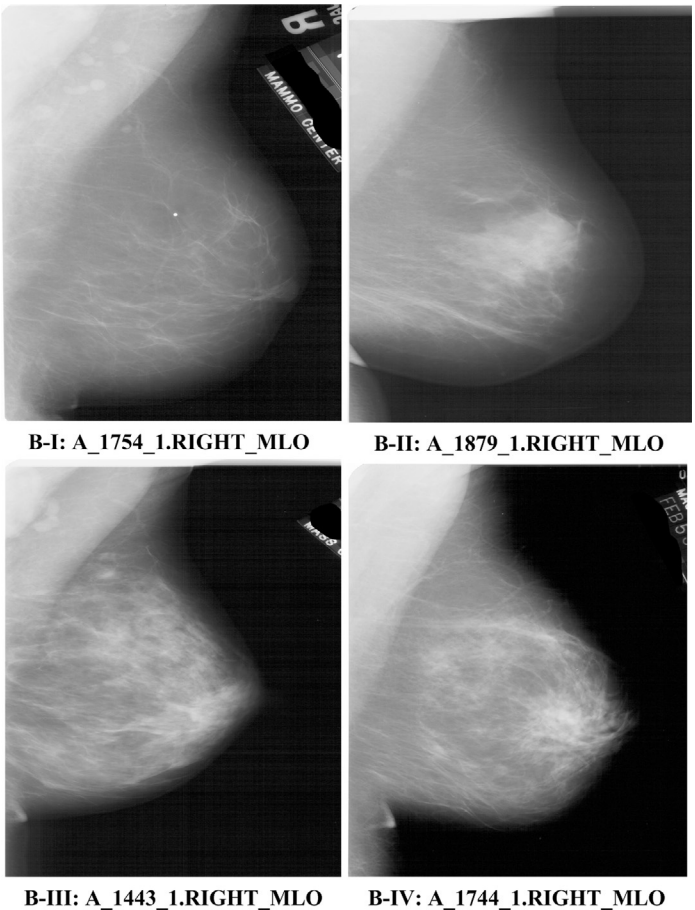

FIG. 1 Sample images of BIRADS classes.

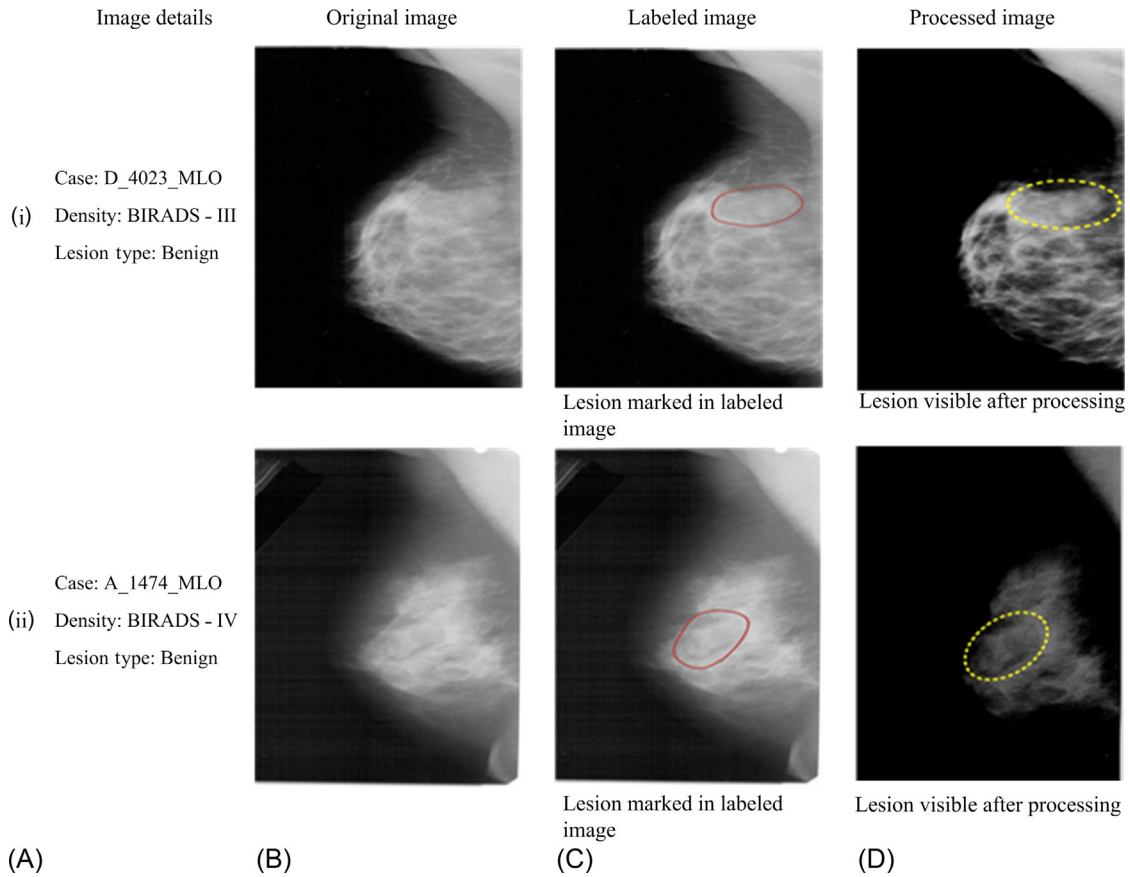

FIG. 2 Sample of dense image in which lesion is behind the glandular ducts. [Note: (A) image details, (B) original image, (C) labeled image, (D) Processed image (lesion is visible after processing)].

However, few studies were performed for 2-class classification of breast density on DDSM dataset based on SBT approach. The maximum accuracy of 96.7% is achieved for 2-class classification of breast density based on SBT approach. It is worth mentioning that no study was conducted for 2-class classification based on ROI approach.

From the Table, it is seen that the greater part of the CAD frameworks utilizes SBT-based approach that incorporates the expulsion of foundation and pectoral muscle [32–36]. This process is highly time consuming, so an ROI-based approach [37–39] can be used as an alternative wherein fixed-size regions of interest (ROI) have been selected from the central area of the mammographic images where maximum density information is present [40].

In the present work, a fixed-size ROI with dimensions 128×128 pixels has been selected from each mammographic image and these ROIs are then used for the computation of texture features. In this work, Laws' mask analysis has been used as the feature extraction technique. The computed features are then passed onto the classification module.

A direct comparison can be drawn between the present study and another study [37–39] used for prediction of breast density as per BIRADS standard.

2 METHODOLOGY ADOPTED

2.1 Depiction of the Dataset

The proposed algorithm has been tested on the mammograms acquired from DDSM dataset. It consists of around 2620 studies with each study including 4 images of the breast (2 mediolateral oblique (MLO) views and 2 craniocaudal (CC) views). There is also some associated information about the patient (like age, rating of abnormality, breast density rating according to ACR determined by an expert radiologist), and image information (type of scanner used, spatial resolution, etc.). In the present work, 480 images (120 images belonging to each BIRADS class) have been considered for analysis [41].

TABLE 1 (A) Description of Studies Performed on DDSM Dataset for 4-Class Classification of Breast Density and (B) Description of Studies Performed on DDSM Dataset for 2-Class Classification of Breast Density

Investigators	SBT/ROI	Classifier	Acc. (%)
(A)			
Bovis et al. [32]	SBT	ANN	71.4
Oliver et al. [33]	SBT	kNN, Decision Tree	47.0
Bosch et al. [34]	SBT	kNN, SVM	84.7
Oliver et al. [35]	SBT	SFS+kNN	77.0
Oliver et al. [36]	SBT	LDA-PCA	94.0
Kumar et al. [37]	ROI	SVM	73.7
Kumar et al. [38]	ROI	HCF	84.6
Kumar et al. [39]	ROI	ANN	90.8
(B)			
Bovis et al. [32]	SBT	ANN	96.7
Oliver et al. [35]	SBT	Bayesian	84.0

Acc.: HCF, hybrid classification framework, Accuracy; ROI, Region of Interest; SBT, Segmented breast tissue.

2.2 ROI Extraction

After acquiring the image, the first step is the extraction of a suitable ROI from the image that is used for further processing. Researchers in a study [40] confirmed the fact that the central section of the breast contains maximum density information. Therefore in this work, ROIs with dimensions 32×32, 64×64, 128×128, and 256×256 pixels are cropped from each mammographic image from the central section of the breast. The process of ROI extraction is depicted in Fig. 3.

For the selection of optimal size of ROI, tedious experimentation has been performed on each ROI size and it was found that the maximum classification accuracy values are obtained for ROI of size 128×128 pixels. Thus, ROI of same size (128×128 pixels) is considered for this work. The results obtained for each ROI are given in Table 2.

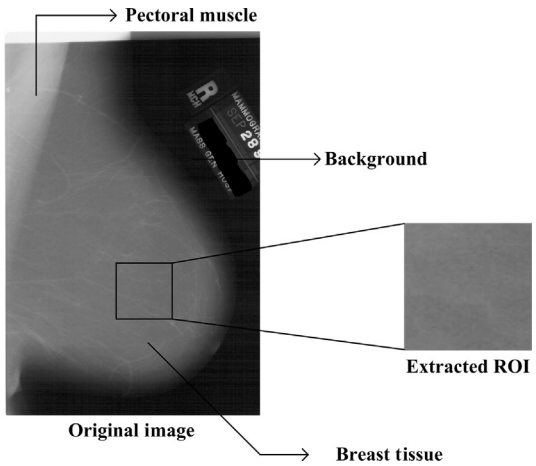

FIG. 3 Process of ROI extraction. Mammographic image B-I: A_2030_1.RIGHT_MLO with ROI marked.

TABLE 2 (A) Results Analysis for ROI Size Selection for 4-Class Problem and (B) Results Analysis for ROI Size Selection for 2-Class Problem

Feature Model	32×32			64×64			128×128			256×256		
	PNN	NFC	SVM	PNN	NFC	SVM	PNN	NFC	SVM	PNN	NFC	SVM
(A)												
Laws3	49.2	50.8	50.1	53.8	54.5	51.5	**65.0**	**65.0**	**64.1**	58.8	61.2	56.2
Laws5	47.8	43.7	50.7	55.8	54.5	49.6	**72.5**	**66.2**	**73.3**	63.4	64.1	70.0
Laws7	50.7	49.5	51.7	57.1	55.4	55.7	**65.2**	**68.7**	**66.2**	65.7	60.5	66.2
Laws9	43.2	37.5	43.2	52.8	53.3	54.6	**62.9**	**61.6**	**69.5**	61.3	56.6	63.3
(B)												
Laws3	81.1	80.8	81.1	82.9	83.3	80.8	**87.5**	**90.0**	**91.2**	84.5	84.1	82.0
Laws5	80.7	77.5	80.7	82.5	82.5	81.7	**87.0**	**89.5**	**89.5**	85.4	85.8	87.9
Laws7	82.8	82.0	82.1	82.0	82.0	84.5	**87.5**	**90.4**	**89.5**	86.2	87.0	87.5
Laws9	78.4	77.0	78.2	82.5	82.5	82.9	**87.5**	**89.5**	**87.5**	85.4	87.0	87.5

2.3 Experimental Workflow

With the improvements in the field of artificial intelligence, a lot of investigators have proposed algorithms for the design of CAD systems that can be useful in the field of medicine as a second opinion tool to the radiologists for characterization of medical images using texture analysis. These tools prove to be assistive in improving the diagnostic accuracy by highlighting the areas of suspicion that may be missed during the visual analysis [42–49].

The general framework of CAD system design is made up of a feature extraction module and a classification module. The experimental workflow for the designing of a computer-assisted classification framework is shown in Fig. 4.

In the present work, the 4-class classification problem can be downsized into a 2-class classification problem by combining together mammographic images of class B-I and class B-II to form "*fatty*" class and mammographic images of class B-III and class B-IV to form "*dense*" class. A description of dataset showing the number of images, ROIs extracted, and bifurcation of data to form training instance and testing instance is revealed in Fig. 5.

From Fig. 4, it is seen that a total of 480 mammographic images have been acquired from the DDSM database. For each BIRADS class (B-I to B-IV), there are 120 mammographic images and from these 120 mammographic images, 120 ROIs are extracted. For 2-class classification, 120 mammographic images of B-I class and 120 mammographic images of B-II class are combined to form "*fatty*" class having 240 mammographic images. Similarly, 120 mammographic images of B-III class are combined with 120 mammographic images of B-IV class to form "*dense*" class having 240 mammographic images.

2.4 Feature Extraction Module

In this module of the CAD system, the underlying texture properties of an image are transformed into mathematical descriptors that can be used to predict the class of the image. Recently, a texture descriptor computed by Laws' method has gained attention for discrimination between different breast tissues [18, 50]. Thus, in this work, Laws' mask analysis has been used for feature extraction by filtering an image with different special 2D masks to compute different texture descriptors that prove to be useful in texture analysis. The basic kernels used in the formation of 2D masks are Level (L), Edge (E), Spot (S), Wave (W), and Ripple (R). The length of these kernels varies as 3, 5, 7, and 9 [24, 50–56]. The description and orientations of these kernels and steps for computing Laws' texture are shown in Fig. 6.

The input feature vectors (IFV) consisting of features computed using different Laws' filters of varying lengths are then fed to (a) Classification Module-1: 4-class PNN classifier, (b) Classification Module-2: 2-class PNN classifier (c) Classification Module-2.1: A 4-class NFC classifier, (d) Classification Module-2.2: A 2-class NFC classifier

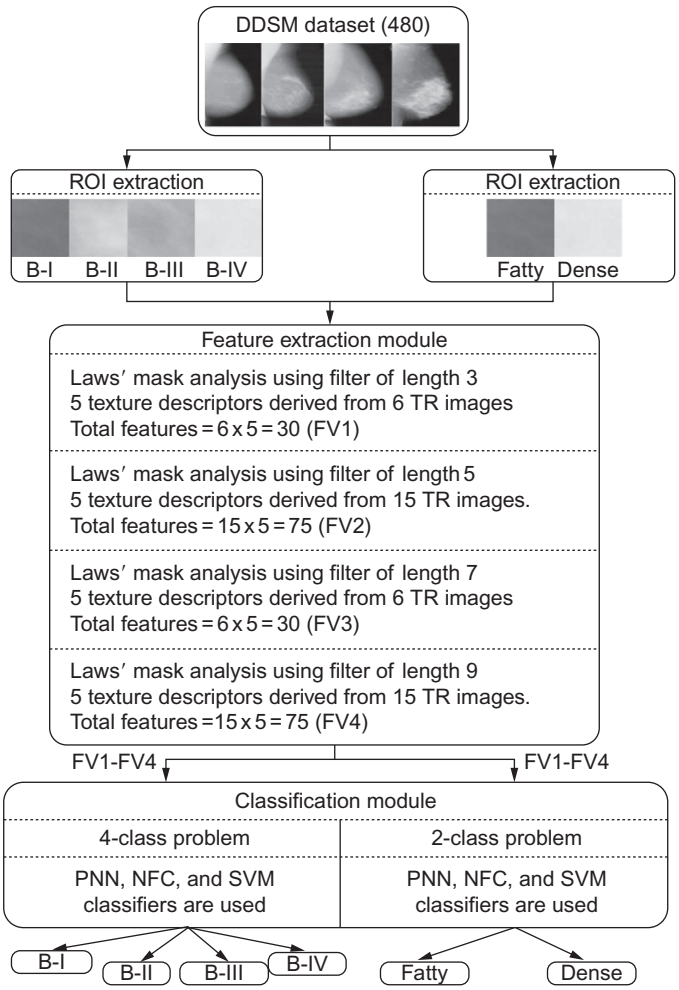

FIG. 4 Experimental workflow for the designing of a computer-assisted classification framework.

(e) Classification Module-3.1: A 4-class SVM classifier and (f) Classification Module-1.2: A 2-class SVM classifier for the classification tasks.

The depiction of the IFVs formed using Laws' mask texture model is given in Table 3.

2.5 Classification Module

The classification module in a CAD system is used to guess the belongingness of an unknown instance to a particular class based on the texture information present in the form of computed IFVs fed to it.

In the present work, two classification modules have been implemented using three classifiers, namely, PNN, NFC, and SVM. Hence, classification module consists of (a) Classification Module-2.1: A 4-class PNN classifier, (b) Classification Module-2.2: A 2-class PNN classifier (c) Classification Module-2.1: A 4-class NFC classifier, (d) Classification Module-2.2: A 2-class NFC classifier, (e) Classification Module-3.1: A 4-class SVM classifier and (f) Classification Module-1.2: A 2-class SVM classifier. The computed IFVs are normalized between [0, 1] by using min-max approximation. A short portrayal of classifiers is given here.

2.5.1 PNN Classifier

The PNN is a sort of neural system classifier that determines the probability of belongingness of an unknown instance to a particular class [57–59] and subsequently called managed neural system classifier. The PNN has a layered architecture consisting of an input layer, a pattern layer, a summation layer, and a decision layer as shown in Fig. 7.

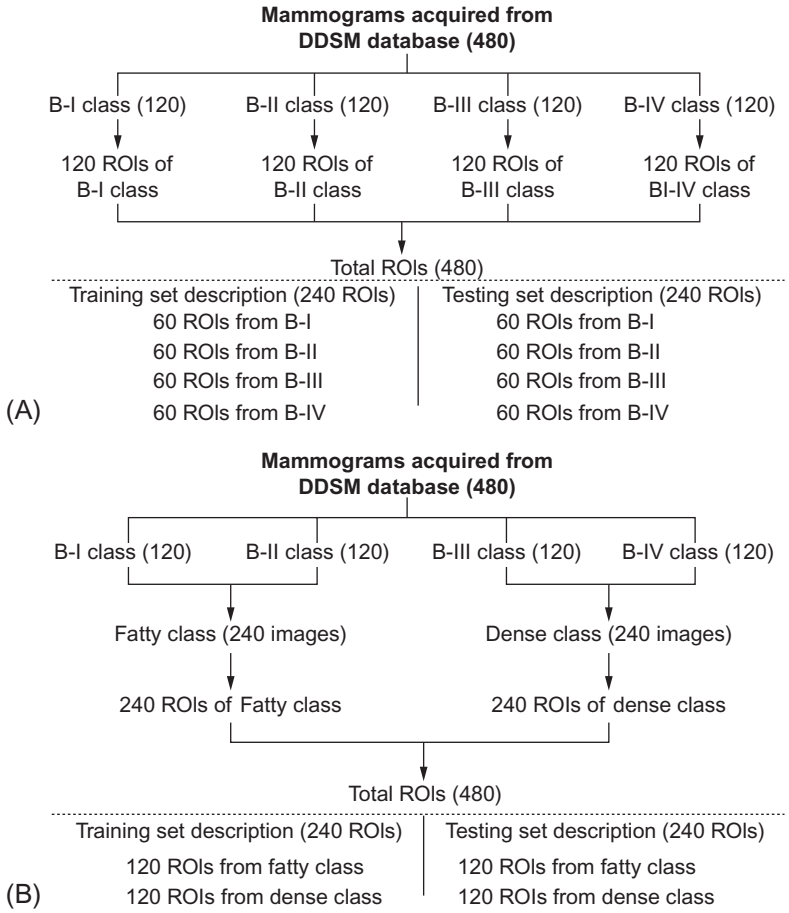

FIG. 5 (A) Description of dataset for 4-class breast density classification and (B) Description of dataset for 2-class breast density classification.

***Input layer*:** The input layer accepts the primitive values of the instance whose class membership is to be decided. It consists of "n" number of neurons. The results obtained from input layer are transferred to a pattern layer, which consists of "p" neurons, "p" being equal to the number of classes.

***Pattern layer*:** The pattern layer contains the probability density function (PDF) belonging to each class that is decided based on the parameter S_p: kernel width parameter or spread parameter and training data.

***Summation layer*:** The qualities from the units in the pattern layer are included in the summation layer to register the reaction of each class. Each of these reactions is thought about in the choice layer and greatest reaction is chosen for each class.

***Decision layer*:** The response collected from the summation layer is compared at this layer and maximum response is opted for every class.

An efficient PNN classifier has been designed on the basis of optimal value of spread parameter S_p that is determined by exhaustive experimentation with $S_p \in \{1, 2, \ldots, 9, 10\}$ using 10-fold cross validation on the instances of training dataset.

2.5.2 NFC Classifier

The NFC is a feed-forward system in light of multilayered engineering that involves different layers, i.e., input layer, membership layer, fuzzification layer, defuzzification layer, normalization layer, and output layer [25,60–70]. After the broad investigation of neural system-based framework and fuzzy inference system-based framework, it was found that fuzzy inference system-based frameworks suffer from the learning capability while the other suffers from the learning capability. Thus, NFC is an outstanding implementation of both, i.e., it overcomes the limited application of neural network and fuzzy inference-based systems. Therefore, the NFC-based systems have the potential to learn and represent knowledge according to defined set of rules and learning ability. The architecture of NFC is shown in Fig. 8 for three classes $\{X_1, X_2, X_3\}$ described using two features $\{\alpha_1, \alpha_2\}$ and every input is defined with three linguistic variables; thus, there are nine fuzzy rules.

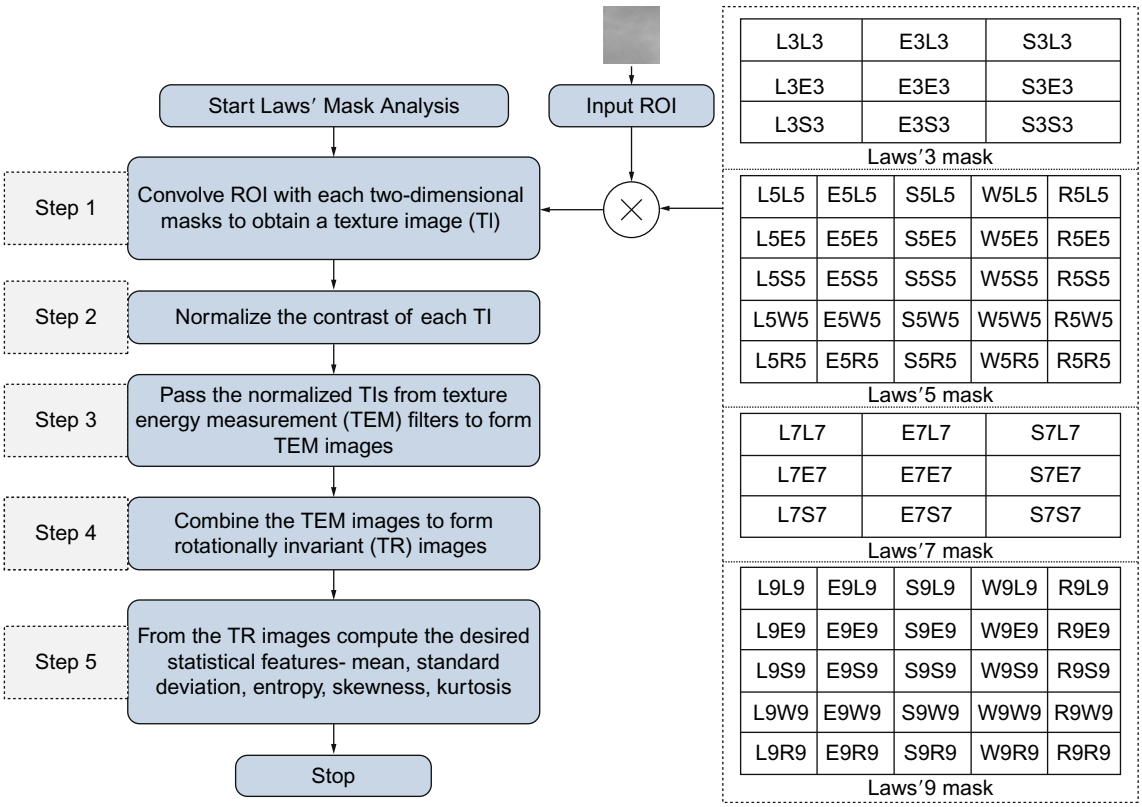

FIG. 6 Steps followed in Laws' mask analysis.

TABLE 3 Description of Laws' Feature Vectors of Different Lengths

IFV	Description	*l*
IFV1	Feature vector formed using Laws' filters of length 3	30
IFV2	Feature vector formed using Laws' filters of length 5	75
IFV3	Feature vector formed using Laws' filters of length 7	30
IFV4	Feature vector formed using Laws' filters of length 9	75

Note: *l*: length of the FV.

Membership layer: There are several types of membership functions that can be used to describe the input variables. In this study, a Gaussian function is used, which is mathematically expressed in Eq. (1).

$$\mu_{ij}(\alpha_{sj}) = e^{-\left(\frac{(\alpha_{sj}-c_{ij})^2}{2\sigma_{ij}^2}\right)} \tag{1}$$

where $\mu_{ij}(\alpha_{sj})$ is the value of membership for ith rule and jth feature; α_{sj} represents the sth sample and jth feature; $\alpha_{sj} - c_{ij}$ represents the central width margin of Gaussian distribution.

Fuzzification layer: This layer generates a firing strength of a fuzzy rule with respect to an object to be classified. The boot strength of the ith rule is calculated by using the Eq. (2).

$$\omega_{ij} = \Pi_{j=1}^{I}(\mu_{ij}(\alpha_{ij})) \tag{2}$$

where I is length of feature space.

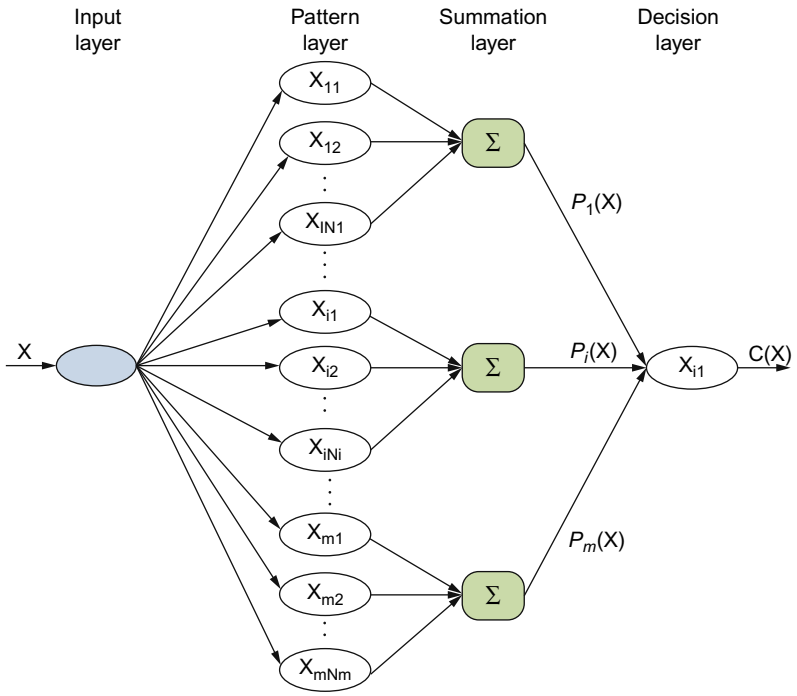

FIG. 7 Architecture of PNN classifier.

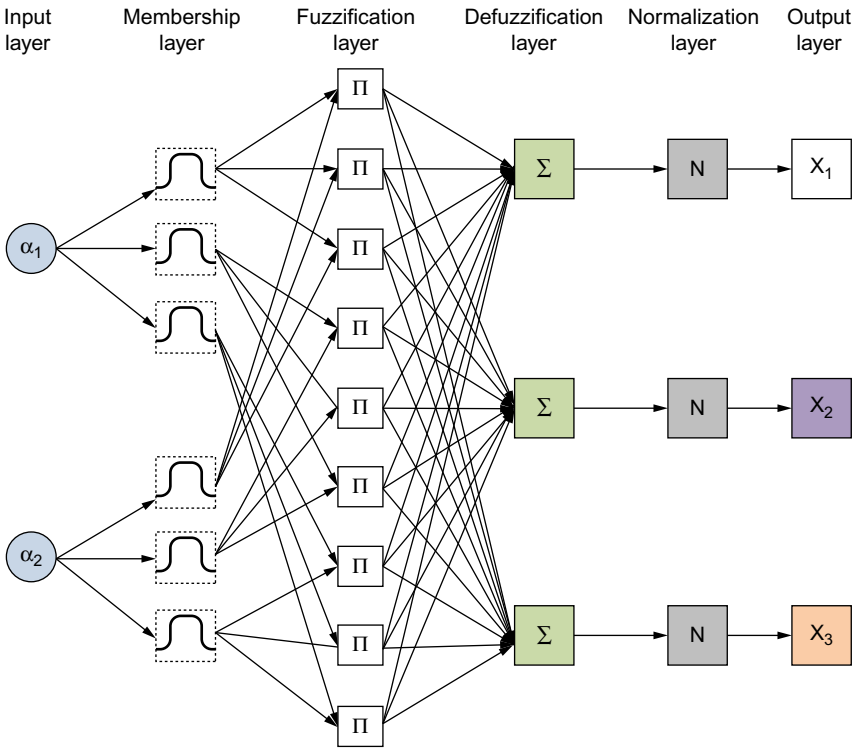

FIG. 8 Architecture of NFC classifier.

Defuzzification layer: This layer calculates the weighted output values for input for each class utilizing the rule sets as per their weights. The weighted output value for a belongingness class is obtained using the Eq. (3).

$$\lambda_{sk} = \sum_{i=1}^{R} \omega_{is} \delta_{ik} \tag{3}$$

Here, δ_{ik} denotes the level of belongingness to the specific kth class that is controlled using ith rule and R represents the number of rules.

Normalization layer: At this layer, the output value should be normalized in the range of {0, 1} using Eq. (4)

$$N_{sk} = \frac{\lambda_{sk}}{\sum_{x=1}^{k} \lambda_{sx}} \tag{4}$$

where N_{sk} denotes the level of having a place with the sth instance of a particular class kth and K is a set of classes. The class label for sth testing instance is predicted by the largest cost of N_{sk} by using Eq. (5).

$$x_s = \max_{k=\{1,2,\ldots,k\}} \{N_{sk}\} \tag{5}$$

The structure used by the NFC for the present work of 4-class classification is shown in Fig. 9.

2.5.3 SVM Classifier

The SVM classifier [70–73] endeavors to build an ideal hyperplane in the higher dimensional component space to isolate the preparation information with least expected risk. The support vector is the instance of data that are closer to the separating hyperplane, and these instances of data lie on the boundary slab as shown in Fig. 10 where + represents the class 1 instance and − represents the class 2 instance.

The various kernel functions are used to design the SVM classifier. The descriptions of the various kernels are given here.

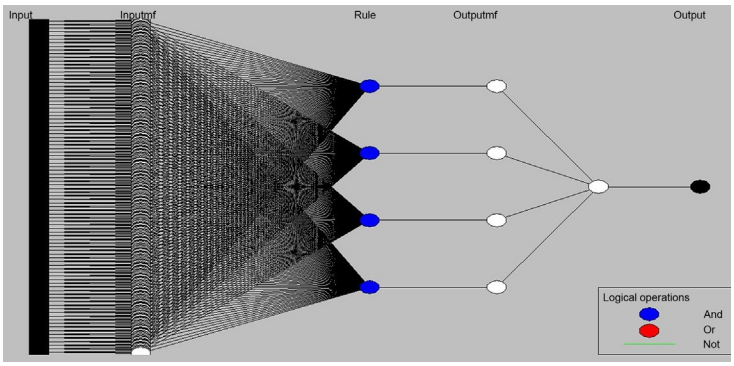

FIG. 9 Designed model based on NFC for 4-class breast density classification.

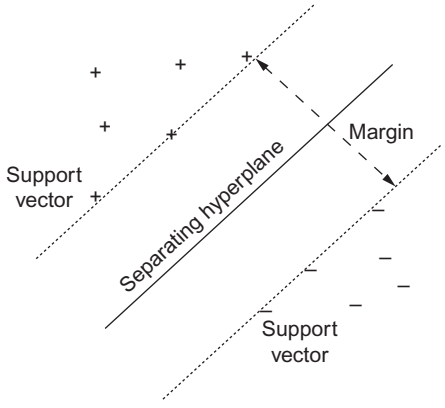

FIG. 10 Representation of support vector and separating hyperplane.

Linear Kernel

The kernel used for creating linear models performs in nonlinear settings, by mapping data to the higher magnitude where it demonstrates linear patterns, by pertaining the linear model in the novel input space. Kernels are the function that returns the significance of the dot product among the images of the two urging.

$$K(a1, a2) = \langle \phi(a1), \phi(a2) \rangle \tag{6}$$

where K is a function; it is feasible to verify that it is a kernel and $a1$, $a2$ are input space.

This is the simplest case of classification. Decision function is a hyperplane in input space. It is valuable to analyze the perceptron algorithm prior to executing SVM. A linear classifier cannot work with the noisy data and nonlinearly separable data. It only covenants with vectorial data. A linear SVM solves the problem by a linear combination of training points.

Quadratic Kernel

Generally, this is a trendy kernel for real-valued vector inputs. The contemplation is to accomplish directly segment by mapping the lower measurement highlight space to a higher dimensional space including nonstraight components, and after that use a straight classifier. Operating in high dimensional feature spaces resolves the difficulty of stating compound functions.

$$k(a, z) = \left(a^T z\right)^2 \tag{7}$$

Polynomial Kernel

In computational theory, the polynomial kernel used with support vector machines (SVMs) characterize the likeness of training data in a component space over polynomials of the first factors, allowing learning of nondirect model. Polynomial kernel is defined as

$$k(a1, a2) = \left(1 + a1^T a2\right)^d \tag{8}$$

Here, $k(a1,a2)$ is a function that contains all polynomial terms up to degree d.

Radial Basis Function Kernel

The RBF kernel used in various kernelized learning algorithms employ infinite dimension feature space and lattice search with crossvalidation. The part of RBF kernel function work connected on two samples a and a', symbolized as feature vectors in some information space, is defined as

$$KER(a, a') = \exp\left(-\frac{\|a - a'\|^2}{2\sigma^2}\right) \tag{9}$$

where $\|a - a'\|^2$ is acknowledged as the Euclidean distance. The Euclidean distance $\|a - a'\|^2$ and σ is known as regularization parameter for RBF kernel function-based SVM classifier. For obtaining the optimal values of regularization parameter, a grid search procedure has been conducted, by evaluating the 10-fold crossvalidation training accuracy for each combination.

Multilayer Perceptron (MLP) Kernel Function

The MLP is a feed-forward artificial neural network system that utilized a back propagation technique and maps sets of information onto a course of action of reasonable yields. An MLP involves various layers of nodes in an organized outline with each layer totally connected with the accompanying one. Apart from the participating nodes, every node is a handling component with a nonlinear activation function [74]. The two fundamental activation functions utilized as a part of current applications are both sigmoid and are depicted by consolidating a few single-layer perceptron. Every single-layer perceptron utilizes a sigmoid-shaped transfer function like the logistic or hyperbolic tangent function.

$$\phi(z) = \tanh(z) \tag{10}$$

$$\phi(z) = \frac{1}{1 + \exp(-z)} \tag{11}$$

In this study, a Gaussian radial basis kernel function-based SVM classifier (available in LibSVM library) has been used for the design of computerized classification framework for breast density classification.

2.5.4 Performance Analysis

The outcome of the designed CAD systems is measured in terms of overall classification accuracy (OCA) and individual class accuracy (ICA). The mathematical expression of the OCA and ICA is given in Eqs. (12), (13), respectively.

$$\text{OCA} = \frac{\text{CC}}{\text{TI}} \times 100 \tag{12}$$

where CC stands for total number of correctly classified instances and TI for total number of testing instances.

$$\text{ICA} = \frac{\text{ICC}}{\text{TIC}} \times 100 \tag{13}$$

where ICC stands for total number of correctly classified instances belonging to a particular class and TIC for total number of testing instances belonging to a particular class.

Cohen's kappa statistical analysis [75] method is used for testing the stability of the designed CAD systems. Suppose that the obtained confusion matrix is given in Fig. 11.

The value of Cohen's kappa is evaluated by using Eq. (14).

$$k = \frac{p_o - p_e}{1 - p_e} \tag{14}$$

where k is known as Cohen's kappa value, p_o is observed accuracy, and p_e is expected accuracy. The value of p_o and p_e is calculated using Eqs. (15), (16), respectively.

$$p_o = \frac{N11 + N22}{N11 + N12 + N21 + N22} \tag{15}$$

$$p_e = \frac{A + B}{N11 + N12 + N21 + N22} \tag{16}$$

where A and B is calculated using Eqs. (17), (18), respectively.

$$A : \text{class/observer1} = (N11 + N12) \times (N11 + N21) \tag{17}$$

$$B : \text{class/observer2} = (N21 + N22) \times (N12 + N22) \tag{18}$$

The significance of the obtained Cohen's kappa value is interpreted according to Fig. 12.

3 EXPERIMENTS AND RESULTS

In the present work, exhaustive experiments were conducted using Laws' mask analysis with different 1D special Laws' filters with an aim to identify the density class of mammographic images according to their texture information cropped

Confusion matrix

		Observer2	
		C1	C2
Observer1	C1	*N*11	*N*12
	C2	*N*21	*N*22

FIG. 11 Confusion matrix (Note: C1, class1; C2, class2).

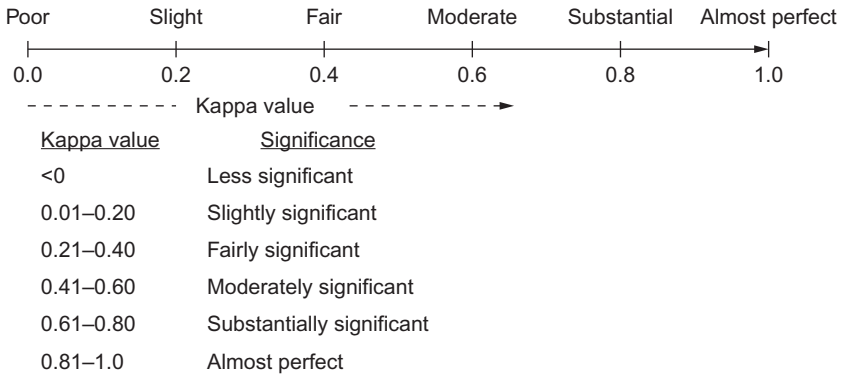

FIG. 12 Significance of the obtained Cohen's kappa value.

from the center area of the mammographic images. The short depiction of the experiments completed for classification of breast density is given in Table 4.

3.1 Experiment 1: Evaluating the Performance of IFV1, IFV2, IFV3, and IFV4 for 4-Class Breast Density Classification Using PNN Classifier

In this examination, the grouping execution of IFV1, IFV2, IFV3, and IFV4 processed utilizing Laws' filters of different lengths has been evaluated for 4-class classification using the probabilistic neural network classifier. The obtained performances of the examination are represented in Table 5.

From the table, it can be inferred that for 4-class classification, the highest OCA achieved is 72.5% with IFV2 formed using features computed by Laws' filter of length 5. For BIRADS class B-I, the ICA value is 63.0%; for class B-II, the ICA value is 100%; for class B-III, the ICA value is 41.60%; and for class B-IV, the ICA value is 85.0%.

It is also observed from the table that the 0.633 is the maximum kappa value using PNN classifier for IFV2. It shows that the designed CAD system using PNN classifier for IFV2 is more significant for clinical purpose than the CAD system designed using IFV1, IFV3, and IFV4.

3.2 Experiment 2: Evaluating the Performance of IFV1, IFV2, IFV3, and IFV4 for 2-Class Breast Density Classification Using PNN Classifier

In this examination, the grouping execution of IFV1, IFV2, IFV3, and IFV4 processed utilizing Laws' filters of different lengths has been evaluated for 2-class classification using the probabilistic neural network classifier. The obtained performances of the examination are represented in Table 6.

It can be inferred from the obtained performances of the examination (Table 6) that for 2-class breast density classification, the OCA achieved is 87.5% with IFV1 and IFV4 formed using features computed by Laws' filters of lengths 3 and 9, respectively. However, the results obtained from IFV1 are considered to be significant as they give comparable OCA to

TABLE 4 Description of the Experiments Carried Out for Classification of Breast Density

Experiment No.	Description
Experiment 1	Evaluating the performance of IFV1, IFV2, IFV3, and IFV4 for 4-class classification using PNN classifier
Experiment 2	Evaluating the performance of IFV1, IFV2, IFV3, and IFV4 for 2-class classification using PNN classification
Experiment 3	Evaluating the performance of IFV1, IFV2, IFV3, and IFV4 for 4-class classification using NFC classifier
Experiment 4	Evaluating the performance of IFV1, IFV2, IFV3, and IFV4 for 2-class classification using NFC classification
Experiment 5	Evaluating the performance of IFV1, IFV2, IFV3, and IFV4 for 4-class classification using SVM classifier
Experiment 6	Evaluating the performance of IFV1, IFV2, IFV3, and IFV4 for 2-class classification using SVM classifier

TABLE 5 Classification Performance of IFVs Computed Using Laws' Mask Analysis for 4-Class Breast Density Classification Using PNN Classifier

IFV	Confusion Matrix					ICA (%)	OCA (%)	Kappa Value
		B-I	B-II	B-III	B-IV			
IFV1	B-I	44	15	1	0	73.3	65.0	0.553
	B-II	17	36	5	2	60.0		
	B-III	0	19	23	18	38.3		
	B-IV	0	1	6	53	88.3		
IFV2	B-I	38	15	7	0	63.3	72.5	0.633
	B-II	0	60	0	0	100		
	B-III	4	19	25	12	41.6		
	B-IV	0	4	5	51	85.0		
IFV3	B-I	45	12	3	0	75.0	61.2	0.483
	B-II	21	29	8	2	48.3		
	B-III	2	19	19	20	31.6		
	B-IV	1	0	5	54	90.0		
IFV4	B-I	40	19	1	0	66.7	61.2	0.483
	B-II	17	38	3	2	63.3		
	B-III	2	22	20	16	33.3		
	B-IV	1	0	10	49	81.6		

TABLE 6 Classification Performance of IFVs Computed Using Laws' Mask Analysis for 2-Class Breast Density Classification Using PNN Classifier

IFVs	Confusion Matrix			ICA (%)	OCA (%)	Kappa Value
		F	D			
IFV1	F	110	10	91.6	87.5	0.750
	D	20	100	83.3		
IFV2	F	115	5	95.8	87.0	0.741
	D	26	94	78.3		
IFV3	F	109	11	90.8	86.2	0.725
	D	22	98	81.6		
IFV4	F	115	5	95.8	87.5	0.750
	D	25	95	79.1		

Note: D, Dense class; F, Fatty class.

those of IFV4 but with considerably lesser number of texture descriptors. The ICA values of 91.6% and 83.3% have been achieved for the "*fatty*" and "*dense*" classes, respectively, using IFV1.

It is also observed that the 0.750 is the maximum kappa value using PNN classifier for IFV1. It shows that the designed CAD system for binary classification problem using PNN classifier for IFV1 is more significant for clinical purpose than CAD system designed using IFV2, IFV3, and IFV4.

3.3 Experiment 3: Evaluating the Performance of IFV1, IFV2, IFV3, and IFV4 for 4-Class Breast Density Classification Using NFC

In this examination, the grouping execution of IFV1, IFV2, IFV3, and IFV4 processed utilizing Laws' filters of different lengths has been evaluated for 4-class classification using the NFC. The obtained performances of the examination are represented in Table 7.

From the table, it can be inferred that for 4-class classification, the highest OCA achieved is 68.7% with IFV3 formed using features computed by Laws' filter of length 7. For BIRADS class B-I, the ICA value is 65.0%; for class B-II, the ICA value is 65.0%; for class B-III, the ICA value is 51.6%; and for class B-IV, the ICA value is 93.3%.

It is also observed that the 0.568 is the maximum kappa value using NFC classifier for IFV3. It shows that the designed CAD system for 4-class classification problem using NFC classifier for IFV3 is more significant for clinical purpose than CAD system designed using IFV1, IFV2, and IFV4.

3.4 Experiment 4: Evaluating the Performance of IFV1, IFV2, IFV3, and IFV4 for 2-Class Breast Density Classification Using NFC

In this examination, the grouping execution of IFV1, IFV2, IFV3, and IFV4 processed utilizing Laws' filters of different lengths has been evaluated for 2-class classification using the NFC classifier. The obtained performances of the examination are represented in Table 8.

It can be inferred from the obtained performances of the examination (Table 7) that for 2-class breast density classification, the OCA achieved is 90.4% with IFV3 formed using features computed by Laws' filters of length 7. The ICA values of 91.6% and 89.1% have been achieved for the "*fatty*" and "*dense*" classes, respectively, using IFV3.

TABLE 7 Classification Performance of IFVs Computed Using Laws' Mask Analysis for 4-Class Breast Density Classification Using NFC Classifier

IFV	Confusion Matrix					ICA (%)	OCA (%)	Kappa Value
		B-I	B-II	B-III	B-IV			
IFV1	B-I	39	19	2	0	65.0	65.0	0.533
	B-II	9	47	2	2	78.3		
	B-III	0	29	15	16	25.0		
	B-IV	0	2	3	55	91.6		
IFV2	B-I	43	10	7	0	71.6	66.2	0.550
	B-II	6	43	7	4	71.6		
	B-III	3	16	23	18	38.3		
	B-IV	5	0	5	50	83.3		
IFV3	B-I	39	19	2	0	65.0	68.7	0.568
	B-II	11	39	9	1	65.0		
	B-III	1	15	31	13	51.6		
	B-IV	0	4	4	56	93.3		
IFV4	B-I	39	6	14	1	65.0	56.6	0.422
	B-II	18	14	26	2	23.3		
	B-III	5	3	36	16	60.0		
	B-IV	5	0	8	47	78.3		

TABLE 8 Classification Performance of IFVs Computed Using Laws' Mask Analysis for 2-Class Breast Density Classification Using NFC Classifier

IFVs	Confusion Matrix			ICA (%)	OCA (%)	Kappa Value
		F	D			
IFV1	F	111	9	92.5	90.0	0.800
	D	15	105	87.5		
IFV2	F	110	10	91.6	89.5	0.791
	D	15	105	87.5		
IFV3	F	110	10	91.6	90.4	0.808
	D	13	107	89.1		
IFV4	F	111	9	92.5	89.5	0.791
	D	16	104	86.6		

It is also observed that the 0.808 is the maximum kappa value using NFC classifier for IFV3. It shows that the designed CAD system for binary classification problem using NFC classifier for IFV3 is more significant for clinical purpose than CAD system designed using IFV1, IFV2, and IFV4.

3.5 Experiment 5: Evaluating the Performance of IFV1, IFV2, IFV3, and IFV4 for 4-Class Breast Density Classification Using SVM Classifier

In this examination, the grouping execution of IFV1, IFV2, IFV3, and IFV4 processed utilizing Laws' filters of different lengths has been evaluated for 4-class classification using the SVM classifier. The obtained performances of the examination are represented in Table 9.

From the table, it can be inferred that for 4-class classification, the highest OCA achieved is 70.8% with IFV2 formed using features computed by Laws' filter of length 5. For BIRADS class B-I, the ICA value is 55.0%; for class B-II, the ICA value is 90.0%; for class B-III, the ICA value is 45.0%, and for class B-IV, the ICA value is 93.3%.

It is also observed that the 0.611 is the maximum kappa value using SVM classifier for IFV2. It shows that the designed CAD system for 4-class classification problem using SVM classifier for IFV2 is more significant for clinical purpose than CAD system designed using IFV1, IFV3, and IFV4.

3.6 Experiment 6: Evaluating the Performance of IFV1, IFV2, IFV3, and IFV4 for 2-Class Breast Density Classification Using SVM Classifier

In this examination, the grouping execution of IFV1, IFV2, IFV3, and IFV4 processed utilizing Laws' filters of different lengths has been evaluated for 2-class classification using the SVM classifier. The obtained performances of the examination are represented in Table 10.

It can be inferred from the obtained performances of the examination (Table 6) that for 2-class breast density classification, the OCA achieved is 91.2% with IFV1 formed using features computed by Laws' filters of length 3. The ICA values of 93.3% and 89.1% have been achieved for the "*fatty*" and "*dense*" classes, respectively, using IFV1.

It is also observed that the 0.825 is the maximum kappa value using SVM classifier for IFV1. It shows that the designed CAD system for binary classification problem using SVM classifier for IFV1 is more significant for clinical purpose than CAD system designed using IFV2, IFV3, and IFV4.

4 CONCLUSION

From the aftereffects of the directed examinations, it can be concluded that for classification of breast density into four classes as per BIRADS standard, features computed from Laws' filters of length 5 are significant in differentiating between

TABLE 9 Classification Performance of IFVs Computed Using Laws' Mask Analysis for 4-Class Breast Density Classification Using SVM Classifier

IFV	Confusion Matrix					ICA (%)	OCA (%)	Kappa Value
		B-I	B-II	B-III	B-IV			
IFV1	B-I	36	19	5	0	60.0	64.1	0.522
	B-II	11	37	10	2	61.6		
	B-III	0	14	29	17	48.3		
	B-IV	0	0	8	52	86.6		
IFV2	B-I	33	21	6	0	55.0	70.8	0.611
	B-II	2	54	2	2	90.0		
	B-III	0	15	27	18	45.0		
	B-IV	1	0	3	56	93.3		
IFV3	B-I	38	20	2	0	63.3	66.2	0.550
	B-II	16	38	4	2	63.3		
	B-III	0	17	26	17	43.3		
	B-IV	0	0	3	57	95.0		
IFV4	B-I	43	15	2	0	71.6	65.0	0.533
	B-II	18	30	10	2	50.0		
	B-III	2	11	30	17	50.0		
	B-IV	2	0	5	53	88.3		

TABLE 10 Classification Performance of IFVs Computed Using Laws' Mask Analysis for 2-Class Breast Density Classification Using SVM Classifier

IFVs	Confusion Matrix			ICA (%)	OCA (%)	Kappa Value
		F	D			
IFV1	F	112	8	93.3	91.2	0.825
	D	13	107	89.1		
IFV2	F	112	8	93.3	90.4	0.808
	D	15	105	87.5		
IFV3	F	103	17	85.8	87.5	0.750
	D	13	107	89.1		
IFV4	F	105	15	87.5	88.7	0.775
	D	12	108	90.0		

the varying breast density patterns, while for classification of breast density into two classes, the features computed from Laws' filters of length 3 are useful in differentiating between the "*fatty*" and "*dense*" classes of the breast tissue.

There are certain cases where the density information cannot be clearly determined solely on subjective analysis, so the CAD systems for breast density classification come into play. In the clinical environment, it is essential for a radiologist to correctly identify the density type of the breast tissue and then double check the mammogram showing a high-density breast

TABLE 11 Classification Performance of Various Classification Modules

Experiment No.	Classifier Used	Accuracy (%)	IFV	Kappa Value
Experiment 1	PNN	72.5	IFV2	0.633
Experiment 2	PNN	87.5	IFV1	0.750
Experiment 3	NFC	68.7	IFV3	0.568
Experiment 4	NFC	90.4	IFV3	0.808
Experiment 5	SVM	70.8	IFV2	0.611
Experiment 6	SVM	91.2	IFV1	0.825

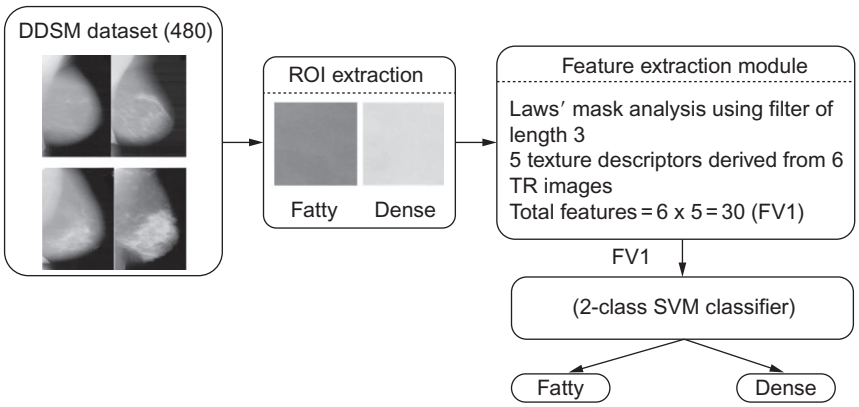

FIG. 13 Proposed CAD system design for breast density classification.

tissue to look for any lesions that might be hidden behind the dense tissue. Using CAD systems for breast density, classification uncertainties that are present at the time of visual analysis can be removed and this also improves the diagnostic accuracy by highlighting certain areas of suspicion that may contain any tumors obscured behind the dense tissue.

The classification performance of various classification modules is summarized in Table 11.

Out of the 4-class breast density classification system and 2-class breast density classification system, the 2-class breast density classification CAD system design is more useful as it gives higher OCA value and ICA value of the dense class, thus indicating that for correctly identifying the breast tissues with high density, a 2-class breast density CAD system can be employed and can prove to be of clinical significance. The proposed CAD system design for breast density classification is shown in Fig. 13.

REFERENCES

[1] K. Ganesan, U.R. Acharya, C.K. Chua, L.C. Min, K.T. Abraham, K.H. Ng, Computer-aided breast cancer detection using mammograms: a review, IEEE Rev. Biomed. Eng. 6 (2013) 77–98.
[2] American Cancer Society, Breast Cancer: Facts and Figures, 2003–04, ACS, Atlanta, 2003.
[3] R.L. Siegel, K.D. Miller, A. Jemal, Cancer statistics, 2015, CA Cancer J. Clin. 65 (1) (2015) 5–29.
[4] J.N. Wolfe, Breast patterns as an index of risk for developing breast cancer, Am. J. Roentgenol. 126 (6) (1976) 1130–1137.
[5] J.N. Wolfe, Risk for breast cancer development determined by mammographic parenchymal pattern, Cancer 37 (5) (1976) 2486–2492.
[6] N.F. Boyd, J.M. Rommens, K. Vogt, V. Lee, J.L. Hopper, M.J. Yaffe, A.D. Paterson, Mammographic breast density as an intermediate phenotype for breast cancer, Lancet Oncol. 6 (10) (2005) 798–808.
[7] N. Boyd, L. Martin, S. Chavez, A. Gunasekara, A. Salleh, O. Melnichouk, M. Yaffe, C. Friedenreich, S. Minkin, M. Bronskill, Breast-tissue composition and other risk factors for breast cancer in young women: a cross-sectional study, Lancet Oncol. 10 (6) (2009) 569–580.
[8] C.M. Vachon, C.H. Van Gils, T.A. Sellers, K. Ghosh, S. Pruthi, K.R. Brandt, V.S. Pankratz, Mammographic density, breast cancer risk and risk prediction, Breast Cancer Res. 9 (6) (2007) 217.
[9] D.S. Mousa, P.C. Brennan, E.A. Ryan, W.B. Lee, J. Tan, C. Mello-Thoms, How mammographic breast density affects radiologists' visual search patterns, Acad. Radiol. 21 (11) (2014) 1386–1393.

[10] N.F. Boyd, G.A. Lockwood, L.J. Martin, J.A. Knight, J.W. Byng, M.J. Yaffe, D.L. Tritchler, Mammographic densities and breast cancer risk, Breast Dis. 10 (3–4) (1998) 113–126.
[11] J.A. Harvey, V.E. Bovbjerg, Quantitative assessment of mammographic breast density: relationship with breast cancer risk 1, Radiology 230 (1) (2004) 29–41.
[12] American College of Radiology, in: American College of Radiology (Ed.), BI-RADS Committee. Breast imaging reporting and data system, American College of Radiology, Reston, VA, 1998.
[13] W.A. Berg, C. Campassi, P. Langenberg, M.J. Sexton, Breast imaging reporting and data system: inter-and intraobserver variability in feature analysis and final assessment, Am. J. Roentgenol. 174 (6) (2000) 1769–1777.
[14] A. Tagliafico, G. Tagliafico, S. Tosto, F. Chiesa, C. Martinoli, L.E. Derchi, M. Calabrese, Mammographic density estimation: comparison among BI-RADS categories, a semi-automated software and a fully automated one, Breast 18 (1) (2009) 35–40.
[15] K. Kerlikowske, D. Grady, J. Barclay, V. Ernster, S.D. Frankel, S.H. Ominsky, E.A. Sickles, Variability and accuracy in mammographic interpretation using the American College of Radiology Breast Imaging Reporting and Data System, J. Natl. Cancer Inst. 90 (23) (1998) 1801–1809.
[16] H.M. Gweon, J.H. Youk, J.A. Kim, E.J. Son, Radiologist assessment of breast density by BI-RADS categories versus fully automated volumetric assessment, Am. J. Roentgenol. 201 (3) (2013) 692–697.
[17] N. Dey, A.S. Ashour, A.S. Althoupety, Thermal imaging in medical science, in: V. Santhi (Ed.), Recent Advances in Applied Thermal Imaging for Industrial Applications, IGI Global, Hershey, PA, 2017, pp. 87–117, https://doi.org/10.4018/978-1-5225-2423-6.ch004.
[18] Kriti, J. Virmani, N. Dey, V. Kumar, PCA-PNN and PCA-SVM based CAD systems for breast density classification, in: A.E. Hassanien, C. Grosan, M. Fahmy Tolba (Eds.), Applications of Intelligent Optimization in Biology and Medicine, Intelligent Systems Reference Library, vol. 96, Springer International Publishing, Cham, 2016, pp. 159–180.
[19] A. Papaevangelou, S. Chatzistergos, K.S. Nikita, G. Zografos, Breast density: computerized analysis on digitized mammograms, Hell. J. Surg. 83 (3) (2011) 133–138.
[20] C. Colin, V. Prince, P.J. Valette, Can mammographic assessments lead to consider density as a risk factor for breast cancer? Eur. J. Radiol. 82 (3) (2013) 404–411.
[21] C. Zhou, H.P. Chan, N. Petrick, M.A. Helvie, M.M. Goodsitt, B. Sahiner, L.M. Hadjiiski, Computerized image analysis: estimation of breast density on mammograms, Med. Phys. 28 (6) (2001) 1056–1069.
[22] J.J. Heine, M.J. Carston, C.G. Scott, K.R. Brandt, W. FF, V.S. Pankratz, T.A. Sellers, C.M. Vachon, An automated approach for estimation of breast density, Cancer Epidemiol. Biomarkers Prev. 17 (11) (2008) 3090–3097.
[23] Z. Huo, M.L. Giger, C.J. Vyborny, Computerized analysis of multiple-mammographic views: Potential usefulness of special view mammograms in computer-aided diagnosis, IEEE Trans. Med. Imaging 20 (12) (2001) 1285–1292.
[24] Z. Tian, N. Dey, A.S. Ashour, P. McCauley, F. Shi, Morphological segmenting and neighborhood pixel-based locality preserving projection on brain MRI dataset for semantic feature extraction: an affective computing study, Neural Comput. Appl. (2017) 1–16, https://doi.org/10.1007/s00521-017-2955-2.
[25] A.M. AlShahrani, M.A. Al-Abadi, A.S. Al-Malki, A.S. Ashour, N. Dey, Automated system for crops recognition and classification, in: N. Dey, A. Ashour, S. Acharjee (Eds.), Applied Video Processing in Surveillance and Monitoring Systems, IGI Global, Hershey, PA, 2017, pp. 54–69, https://doi.org/10.4018/978-1-5225-1022-2.ch003.
[26] S. Goswami, U. Dey, P. Roy, A. Ashour, N. Dey, Medical Video Processing: Concept and Applications, in: N. Dey, A. Ashour, P. Patra (Eds.), Feature Detectors and Motion Detection in Video Processing, IGI Global, Hershey, PA, 2016, pp. 1–17, https://doi.org/10.4018/978-1-5225-1025-3.ch001.
[27] S.C. Satapathy, N. Sri Madhava Raja, V. Rajinikanth, A.S. Ashour, N. Dey, Multi-level image thresholding using Otsu and chaotic bat algorithm, Neural Comput. Appl. (2016) 1–23, https://doi.org/10.1007/s00521-016-2645-5.
[28] S. Hore, S. Chatterjee, S. Sarkar, N. Dey, A.S. Ashour, D. Balas-Timar, V.E. Balas, Neural-based prediction of structural failure of multistoried RC buildings, Struct. Eng. Mech. 58 (3) (2016) 459–473.
[29] L. Saba, N. Dey, A.S. Ashour, S. Samanta, S.S. Nath, S. Chakraborty, J. Sanches, D. Kumar, R. Marinho, J.S. Suri, Automated stratification of liver disease in ultrasound: an online accurate feature classification paradigm, Comput. Methods Prog. Biomed. 130 (2016) 118–134.
[30] S. Chatterjee, S. Sarkar, S. Hore, N. Dey, A.S. Ashour, V.E. Balas, Particle swarm optimization trained neural network for structural failure prediction of multistoried RC buildings, Neural Comput. Appl. (2016) 1–2.
[31] N. Dey, A. Ashour (Eds.), Classification and clustering in biomedical signal processing, IGI Publishing, Hershey, PA, USA, 2016, ISBN: 1522501401 9781522501404.
[32] K. Bovis, S. Singh, in: Classification of mammographic breast density using a combined classifier paradigm, In 4th international workshop on digital mammography Jul 22, 2002, pp. 177–180.
[33] M. Mustra, M. Grgic, K. Delac, in: Feature selection for automatic breast density classification, ELMAR, 2010 PROCEEDINGS Sep 15 (pp. 9–16). IEEE, 2010.
[34] A. Bosch, X. Munoz, A. Oliver, J. Marti, in: Modeling and classifying breast tissue density in mammograms, Computer Vision and Pattern Recognition, IEEE Computer Society Conference on 2006 (Vol. 2, pp. 1552–1558). IEEE, 2006.
[35] A. Oliver, J. Freixenet, R. Marti, J. Pont, E. Perez, E.R. Denton, R. Zwiggelaar, A novel breast tissue density classification methodology, IEEE Trans. Inf. Technol. Biomed. 12 (1) (2008) 55–65.
[36] A. Oliver, X. Lladó, E. Pérez, J. Pont, E.R. Denton, J. Freixenet, J. Martí, A statistical approach for breast density segmentation, J. Digit. Imaging 23 (5) (2010) 527–537.

[37] I. Kumar, H.S. Bhadauria, J. Virmani, Wavelet packet texture descriptors based four-class BIRADS breast tissue density classification, Procedia Comput. Sci. 70 (2015) 76–84.
[38] I. Kumar, H.S. Bhadauria, J. Virmani, S. Thakur, A classification framework for prediction of breast density using an ensemble of neural network classifiers, Biocybern. Biomed. Eng. 37 (1) (2017) 217–228.
[39] I. Kumar, H.S. Bhadauria, J. Virmani, S. Thakur, A hybrid hierarchical framework for classification of breast density using digitized film screen mammograms, Multimed. Tools Appl. 76 (2017) 18789–18813, https://doi.org/10.1007/s11042-016-4340-z.
[40] H. Li, M.L. Giger, Z. Huo, O.I. Olopade, L. Lan, B.L. Weber, I. Bonta, Computerized analysis of mammographic parenchymal patterns for assessing breast cancer risk: effect of ROI size and location, Med. Phys. 31 (3) (2004) 549–555.
[41] M. Heath, K. Bowyer, D. Kopans, R. Moore, W.P. Kegelmeyer, in: The digital database for screening mammography, 5th International Workshop on Digital Mammography Jun 11 (pp. 212–218). Medical Physics Publishing, 2000.
[42] J. Tang, R.M. Rangayyan, J. Xu, I. El Naqa, Y. Yang, Computer-aided detection and diagnosis of breast cancer with mammography: recent advances, IEEE Trans. Inf. Technol. Biomed. 13 (2) (2009) 236–251.
[43] K. Doi, Computer-aided diagnosis in medical imaging: historical review, current status and future potential, Comput. Med. Imaging Graph. 31 (4) (2007) 198–211.
[44] K. Doi, H. MacMahon, S. Katsuragawa, R.M. Nishikawa, Y. Jiang, Computer-aided diagnosis in radiology: potential and pitfalls, Eur. J. Radiol. 31 (2) (1999) 97–109.
[45] M.L. Giger, K. Doi, H. MacMahon, R.M. Nishikawa, K.R. Hoffmann, C.J. Vyborny, R.A. Schmidt, H. Jia, K. Abe, X. Chen, A. Kano, S. Katsuragawa, F.F. Yin, N. Alperin, C.E. Metz, F.M. Behlen, D. Sluis, An intelligent workstation for computer-aided diagnosis, Radiographics 3 (1993) 647–656.
[46] H. Li, M.L. Giger, O.I. Olopade, A. Margolis, L. Lan, M.R. Chinander, computerized texture analysis of mammographic parenchymal patterns of digitized mammograms 1, Acad. Radiol. 12 (7) (2005) 863–873.
[47] I. Kumar, J. Virmani, H.S.A. Bhadauria, in: Review of breast density classification methods, 2nd IEEE International Conference on Computing for Sustainable Global Development, (IndiaCom-2015) (pp. 1960-1967). IEEE, 2015.
[48] G.D. Tourassi, Journey toward computer-aided diagnosis: role of image texture analysis 1, Radiology 213 (2) (1999) 317–320.
[49] H.P. Chan, K. Doi, C.J. Vybrony, R.A. Schmidt, C.E. Metz, K.L. Lam, T. Ogura, Y. Wu, H. MacMahon, Improvement in radiologists' detection of clustered microcalcifications on mammograms: the potential of computer-aided diagnosis, Investig. Radiol. 25 (10) (1990 Oct 1) 1102–1110.
[50] Kriti, J. Virmani, Breast density classification using Laws' mask texture features, Int. J. Biomed. Eng. Technol. 19 (3) (2015) 279–302.
[51] N. Dey, A.S. Ashour, A.E. Hassanien, Feature detectors and descriptors generations with numerous images and video applications: a recap, in: N. Dey, A. Ashour, P. Patra (Eds.), Feature Detectors and Motion Detection in Video Processing, IGI Global, Hershey, PA, 2017, pp. 36–65, https://doi.org/10.4018/978-1-5225-1025-3.ch003.
[52] L. Moraru, S. Moldovanu, L.T. Dimitrievici, A.S. Ashour, N. Dey, Texture anisotropy technique in brain degenerative diseases, Neural Comput. Appl. (2016) 1–11.
[53] G.H. Seng, H.Y. Chai, T.T. Swee, Research on Laws' mask texture analysis system reliability, Res. J. Appl. Sci. Eng. Technol. 7 (19) (2014) 4002–4007.
[54] K.I. Laws, in: Rapid texture identification, 24th annual technical symposium Dec 23 (pp. 376–381). International Society for Optics and Photonics, 1980.
[55] S.G. Mougiakakou, S. Golimati, I. Gousias, A.N. Nicolaides, K.S. Nikita, Computer–aided diagnosis of carotid atherosclerosis based on ultrasound image statistics, Laws' texture and neural networks, Ultrasound Med. Biol. 33 (2007) 26–36.
[56] M. Rachidi, A. Marchadier, C. Gadois, E. Lespessailles, C. Chappard, C.L. Benhamou, Laws' masks descriptors applied to bone texture analysis: an innovative and discriminant tool in osteoporosis, Skelet. Radiol. 37 (6) (2008) 541–548.
[57] D.F. Specht, Probabilistic neural networks, Neural Netw. 3 (1) (1990) 109–118.
[58] V.L. Georgiou, N.G. Pavlidis, K.E. Parsopoulos, P.D. Alevizos, M.N. Vrahatis, in: Optimizing the performance of probabilistic neural networks in a bioinformatics task, Proceedings of the EUNITE 2004 Conference, 2004, pp. 34–40.
[59] D.F. Specht, H. Romsdahl, in: Experience with adaptive probabilistic neural networks and adaptive general regression neural networks, Neural Networks, 1994. IEEE World Congress on Computational Intelligence., IEEE International Conference on 1994 Jun (Vol. 2, pp. 1203–1208). IEEE, 1994.
[60] R. Kher, T. Pawar, V. Thakar, H. Shah, Physical activities recognition from ambulatory ECG signals using neuro-fuzzy classifiers and support vector machines, J. Med. Eng. Technol. 39 (2) (2015) 138–152.
[61] B. Cetişli, A. Barkana, Speeding up the scaled conjugate gradient algorithm and its application in neuro-fuzzy classifier training, Soft. Comput. 14 (4) (2010) 365–378.
[62] S. Kar, S. Das, P.K. Ghosh, Applications of neuro fuzzy systems: a brief review and future outline, Appl. Soft Comput. 15 (2014) 243–259.
[63] S.S. Ahmed, N. Dey, A.S. Ashour, D. Sifaki-Pistolla, D. Bălas-Timar, V.E. Balas, J.M. Tavares, Effect of fuzzy partitioning in Crohn's disease classification: a neuro-fuzzy-based approach, Med. Biol. Eng. Comput. 55 (1) (2017) 101–115.
[64] Li, Z., Shi, K., Dey, N., Ashour, A.S., Wang, D., Balas, V.E., McCauley, P. and Shi, F., Rule-based back propagation neural networks for various precision rough set presented KANSEI knowledge prediction: a case study on shoe product form features extraction. Neural Comput. Appl., pp. 1-18.
[65] C.T. Sun, J.S. Jang, A neuro-fuzzy classifier and its applications, in: Fuzzy Systems, Second IEEE International Conference on 1993 (pp. 94–98). IEEE, 1993.
[66] R. Fuller, Neural Fuzzy Systems, Abo Akademi University, Turku, 1995, ISBN: 951-650-624-0.

[67] S. Khalifa, M.H. Komarizadeh, An intelligent approach based on adaptive neuro-fuzzy inference systems (ANFIS) for walnut sorting, Aust. J. Crop. Sci. 6 (2) (2012) 183.
[68] A. Stepnowski, M. Moszyński, T. Van Dung, Adaptive neuro-fuzzy and fuzzy decision tree classifiers as applied to seafloor characterization, Acoust. Phys. 49 (2) (2003) 193–202.
[69] I.F. Iatan, S. Grunwald, A neuro-fuzzy approach to classification of ECG signals for ischemic heart disease diagnosis, AMIA Ann. Symp. Proc. (2003) 494–498.
[70] L.P. Bhaiya, V.K. Verma, Classification of MRI brain images using neural network, Int. J. Eng. Res. Appl. 2 (5) (2012) 751–756.
[71] C.C. Chang, C.J. Lin, LIBSVM, A library of support vector machines, Available from, http://www.csie.ntu.edu.tw/∼cjlin/libsvm, 2012.
[72] A.E. Hassanien, N.E. Bendary, M. Kudelka, V. Snasel, in: Breast cancer detection and classification using support vector machines and pulse coupled neural network, 3rd International Conference on Intelligent Human Computer Interaction 'IHCI 2011'. pp. 269–79, 2011.
[73] A.T. Azar, S.A. El-Said, Performance analysis of support vector machines classifiers in breast cancer mammography recognition, Neural Comput. Appl. 24 (5) (2014) 1163–1177.
[74] N. Cristianini, J. Shawe-Taylor, An Introduction to Support Vector Machines and Other Kernel-Based Learning Methods, Cambridge University Press, Cambridge, 2000, Mar 23, ISBN: 0521780195.
[75] A.J. Viera, J.M. Garrett, Understanding interobserver agreement: the kappa statistic, Fam. Med. 37 (5) (2005) 360–363.